

DANISH METEOROLOGICAL INSTITUTE

————— **SCIENTIFIC REPORT** —————

04-02

**Error Analyses of Refractivity Profiles Retrieved from
CHAMP Radio Occultation Data**

Andrea K. Steiner



Copenhagen 2004

ISSN 0905-3263 (print)
ISSN 1399-1949 (online)
ISBN 87-7478-499-4

Error Analyses of Refractivity Profiles Retrieved from CHAMP Radio Occultation Data

Andrea K. Steiner

Atmosphere Ionosphere Research Division
Danish Meteorological Institute, 2100 Copenhagen, Denmark

August 2003

Abstract. The objective of this study was the empirical error analysis and the comparison of a set of refractivity profiles retrieved from CHAMP (CHALLENGING Minisatellite Payload) radio occultation observations. The data set comprises one week of observations, January 1–7, 2003, with about 1200 radio occultation profiles. We compared refractivity profiles based on geometric optics retrievals of three different retrieval schemes including the GRAS SAF prototype retrieval of DMI (Danish Meteorological Institute, Copenhagen), the operational retrieval of GFZ (GeoForschungsZentrum, Potsdam), and the EGOPS/CC retrieval of IGAM (Institute for Geophysics, Astrophysics, and Meteorology, Graz). The error statistics is based on the comparison of the retrieved profiles with co-located refractivity profiles calculated from ECMWF (European Centre for Medium-range Weather Forecasts) analyses fields. Overall, quite consistent results are found for the three different retrieval schemes, showing a bias of about -0.3% at 5–25 km height with respect to ECMWF. The standard deviation is about 0.5–1% at 5–30 km height for the DMI and the GFZ retrieval, respectively. The IGAM retrieval shows a larger standard deviation of up to 1.5% above 20 km height. Differences in the error characteristics are most pronounced above 30 km height which can be attributed to the differences in the retrieval schemes, most probably to the bending angle initialization. The results are consistent with the findings of Wickert et al. (2003a; 2003b) and Kuo et al. (2003). Furthermore error correlation functions were analyzed showing consistency with respect to those derived in a simulation study by Steiner and Kirchengast (2003a). The provided error characteristics are an estimate of the upper error level since they contain both, the observational error of the retrieved data and the model error of the ECMWF analyses. The thorough estimation of the ECMWF model error is subject to near future work. This will allow the separation of the observation error and the specification of proper observation error covariance matrices for data assimilation systems. Meanwhile the simple error covariance model based on the simulation study results (Steiner and Kirchengast, 2003a; 2003b) adjusted to the error magnitude of the respective observing and retrieval system seems to be a quite useful approximation.

1 Introduction

The assimilation of radio occultation data has the potential to significantly improve the accuracy of global and regional meteorological analysis and weather prediction which has been confirmed by several studies (e.g., Kuo et al., 2000; Healy et al., 2003). One important issue in this respect is the knowledge on radio occultation measurement errors in order to formulate proper observation error covariance matrices for data assimilation systems.

Since refractivity seems to be the most appropriate parameter for assimilation purposes we performed an empirical error analysis of a set of refractivity profiles retrieved from CHAMP radio occultation observations. Three different data processing schemes were compared and analyzed including the refractivity retrievals of GFZ (Potsdam), DMI (Copenhagen), and IGAM (Graz). The error statistics is based on comparison to reference profiles calculated from ECMWF analyses fields. This implies that the error statistics includes both, the observation error and the ECMWF model error. Since we do not yet have realistic error estimates for the ECMWF model error in order to separate it from the observation error we provide an estimate of the upper error level for refractivity.

We analyze refractivity error characteristics comprising bias, standard deviation and error correlation functions. The results of this study are compared to the findings of Wickert et al. (2003a; 2003b) and Kuo et al. (2003) who analyzed CHAMP and SAC-C (Satelite de Aplicaciones Cientificas-C) data. We also compare to the results of a simulation study on empirical error characteristics of radio occultation data which is the precursor of this work (Steiner and Kirchengast, 2003a; 2003b).

Section 2 gives a description of the data set and the retrieval algorithms. In Sec. 3 the error statistics calculation is described. The results of the error statistics are described in Sec. 4 for the three different retrieval schemes. A comparison and discussion of the results is given in Sec 5. Summary and conclusions are drawn in Sec. 6.

2 Description of the Data Set and Retrieval Schemes

This study is based on a CHAMP level 2 data set comprising one week of radio occultation observations, January 1–7, 2003, with 1253 profiles of atmospheric excess phases in total. The data are available from the CHAMP Information System and Data Center at GFZ Potsdam (<http://isdc.gfz-potsdam.de/champ>). A comprehensive description of the CHAMP data processing is given by Wickert et al. (2003a; <http://www.gfz-potsdam.de/gasp>).

Refractivity profiles were calculated from this data base of excess phase profiles by using three different processing schemes:

- The operational retrieval (version 4) of GFZ Potsdam, CHAMP level 3 data,
- the GRAS SAF (Global navigation satellite system Receiver for Atmospheric Sounding Science Application Facility) prototype retrieval of DMI, Copenhagen, and,
- the EGOPS/CC (End-to-end GNSS Occultation Performance Simulator/CHAMPCLIM) retrieval version 1 of IGAM, Graz.

All three retrieval schemes are based on the standard geometric optics approach for the calculation of bending angle profiles and on the Abel inversion technique for the calculation of refractivity profiles (see e.g., Hocke, 1997; Steiner et al., 1999). Basically, the processing chain from excess phases via bending angles to refractivity involves smoothing of the data, an ionospheric correction scheme, the initialization of the measured

bending angle profiles, and a quality control. Table 1 gives an overview on the refractivity retrieval schemes of GFZ, DMI and IGAM with respect to the implementation of these processing steps.

Smoothing in the GFZ retrieval is performed with a sliding window over 90 data points while DMI and IGAM apply a regularization routine (Syndergaard, 1999).

In all three retrievals an ionospheric correction of bending angles (Vorob'ev and Krasil'nikova, 1994) is performed while slight differences in the extrapolation of bending angles in the troposphere exist (see Table 1).

The measured bending angle profiles are initialized with background bending angle profiles stemming from the MSISE-90 model (Hedin, 1991) which is used by GFZ, DMI and IGAM. GFZ performs a statistical bending angle optimization with inverse variance weighting following the scheme of Sokolovskiy and Hunt (1996). The error in the bending angle is estimated for each observation between 60–70 km using noise analyses. The model bending angle error of the MSISE-90 climatology is set to 20%. DMI has implemented the heuristic bending angle optimization method proposed by Hocke (1997) constraining the data profile with a model profile from the MSIS90_DMI model (Syndergaard, 1999) above 45 km. They use a best fit model bending angle after performing a zonal band search and a longitudinal search in the MSISE90_DMI model data base. In the IGAM retrieval a best fit model bending angle using a global search algorithm in the MSISE-90 model data base with an empirical background bias correction (Gobiet, 2003) is used. A statistical optimization with inverse covariance weighting after Healy (2001) is applied using vertical error correlation with the background bending angle error set to 15% and the measured bending angle error estimated above 60 km.

The GFZ quality control is based on a comparison with ECMWF analyses. The refractivity profile is rejected if at least one data point shows more than 10% in fractional difference between 8–35 km. Below 8 km the refractivity profile is cut off if the fractional difference exceeds 10%. DMI and IGAM have an intrinsic quality control where the profile is cut off when large impact parameter ambiguities occur. The DMI quality check requires continuous data between 10–45 km. IGAM additionally compares to ECMWF analyses rejecting refractivity profiles with more than 10% in fractional difference.

For this study the global ensembles were analyzed and in addition the data sets were separated into three latitude bands, low (-30° to $+30^{\circ}$), middle ($\pm 30^{\circ}$ to $\pm 60^{\circ}$), and high ($\pm 60^{\circ}$ to $\pm 90^{\circ}$) latitudes. The total number of refractivity profiles is different for each retrieval scheme due to the different implementation of the above described processing steps. Especially, the implemented quality checks with its cut-off criterions determine the 'length' of the profiles and thus the number of data points in the troposphere going into the error analyses. GFZ provides a total number of 1253 refractivity profiles (100%) corresponding to the number of excess phase profiles (level 2 data), the IGAM retrieval gives 1184 (~94%) and the DMI retrieval 1038 (83%) refractivity profiles, respectively. Instead of using the 1253 original profiles of GFZ we restricted to the number of IGAM retrievals. Thus, the number of profiles for GFZ in this study is exactly the same as for IGAM in order to be consistent in the interpretation of the results. For technical reasons we could not adjust the number of profiles to be the same for all three data sets.

Retrieval Steps	GFZ Operational Retrieval Version 4, Jul. 2003	IGAM EGOPS/CC Retrieval Version 1, Jul. 2003	DMI GRASSAF Prototype Jul. 2003
Smoothing	Smoothing via 90 data points	Smoothing using regularization (third order norm, regularization parameter = $10^{(\text{Sampling rate}/10)}$ (Syndergaard 1999)	Down-sampled to 10 Hz using the average of the 5 neighbor points. Smoothing using regularization, regularization parameter = 10^4
Ionospheric Calibration	Linear combination of bending angles (α_1, α_2) (Vorob'ev and Krasil'nikova, 1994) $<12\text{km}: \alpha_2' = \alpha_1 + \Delta\alpha$ $\Delta\alpha$ is mean difference (via 4 km) between α_1 and α_2 at 12 km, the transition between α_2 and α_2' is done "smooth" between 12 – 8 km (\cos^2 weighted combination of α_2 and α_2' , 100% α_2 at 12 km, 100% α_2' at 8 km)	Linear combination of bending angles (Vorob'ev and Krasil'nikova, 1994). L2 bending angles < 15 km are derived via L1-L2 extrapolation.	Linear combination of bending angles. L2 bending angles < 10 km are derived via L1-L2 extrapolation.
Bending Angle Initialization	Bending angle optimized (Sokolovskiy and Hunt, 1996), with MSISE-90 (Hedin, 1991), estimation of the observation error for each occultation using noise analyses between 60 – 70 km, and a model bending angle error of 20%.	Statistical Optimization (inverse covariance weighting, Healy 2001) up to 120 km. Between topmost observed data point and 120 km: 100% background information. Vertically correlated background- (correlation length $L=6$ km) and observation- ($L=1$ km) errors. Observation error estimated from observed profile above 60 km for measured CHAMP data. Background error: 15%. Background information source: MSISE90-based bending angle profiles (Hedin, 1991), empirical background bias correction (Gobiet 2003).	Statistical optimization (Hocke 1997) constraining the data profile with a model profile from the MSIS90_DMI model (Syndergaard, 1999) above 45 km. At 60 km the bending angles are set to be identical to the model profile. The model profile is found from the MSIS90_DMI bending angle model as a best fit between 45 and 75 km, doing a zonal band search at +/-15 deg around the tangent point latitude (every 1 deg) and for all longitudes (every 5 deg).
Quality Control	10% in fractional refractivity ECMWF 8–35 km: profile rejected <8 km: profile cut off	Intrinsic quality control: Lower part of profile is cut off when large impact parameter ambiguities occur (only in GO retrieval). Criteria for quality control with reference data: 5–35 km: 10% refractivity; 8–25 km: 25 K temperature. Reference: ECMWF analysis	Intrinsic quality control: Lower part of profile is cut off when large impact parameter ambiguities occur. All profiles must contain continuous data between 10 and 45 km.

Table 1. Implementation of different processing steps from data smoothing, ionospheric calibration, initialization of bending angles to quality control in the refractivity retrievals of GFZ, DMI, and IGAM.

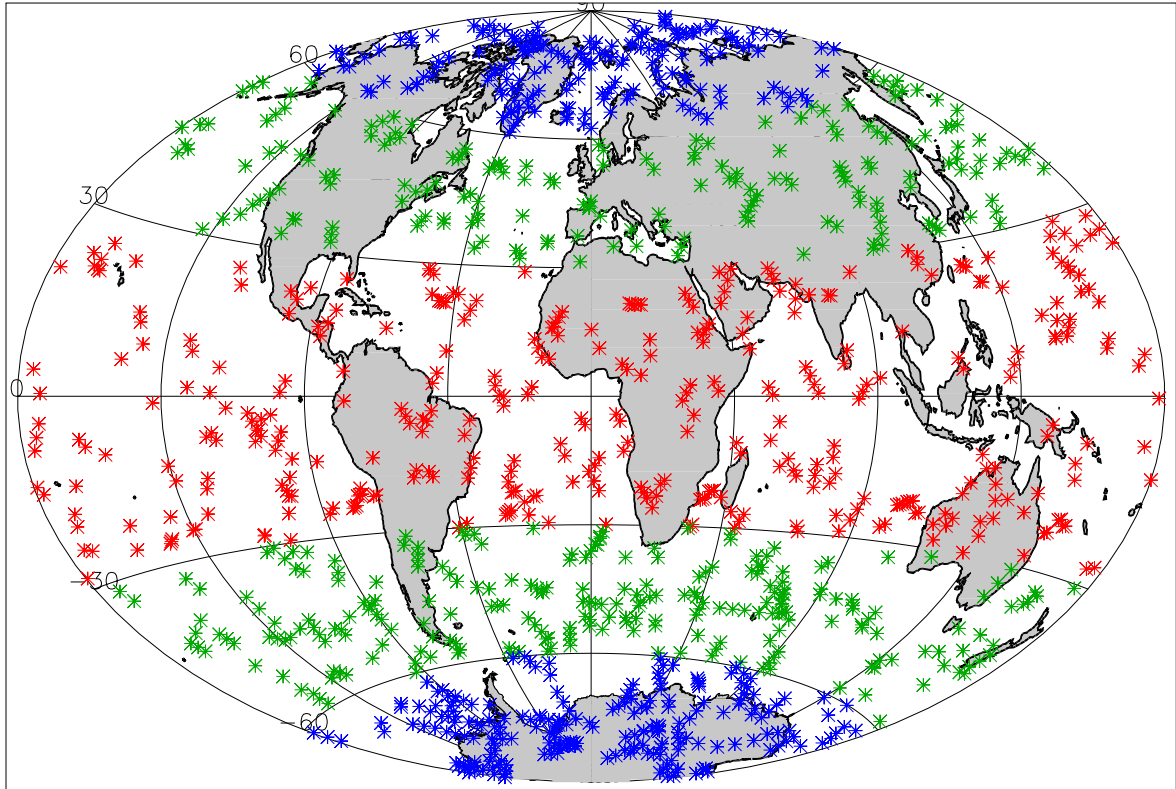


Fig. 1. Distribution of 1184 refractivity profiles from CHAMP occultation observations for January, 1–7, 2003, using the IGAM retrieval. The latitudinal circles show the separation into three latitude bands, low (-30° to $+30^\circ$), middle ($\pm 30^\circ$ to $\pm 60^\circ$), and high ($\pm 60^\circ$ to $\pm 90^\circ$) latitudes.

The profiles are almost equally distributed over the globe with 371/323, 430/379, and 383/336 profiles for GFZ-IGAM / DMI in low, mid-, and high latitudes, respectively. Figure 2 gives an overview on the total number of profiles used for the following analyses. The number of profiles for the ensemble statistics decreases with decreasing height giving at the lowest heights 73/64 profiles for the GFZ-IGAM / DMI retrieval globally and only 12 profiles in the low latitude ensembles. This is illustrated in Fig. 3 showing the number of events for the different data ensembles as a function of height up to 20 km, above this height the number of profiles is constant. The height at which more than 50% of the events are available for the error statistics is varying from ~ 2.5 km in high latitudes, to ~ 5 km in mid latitudes and for the global ensemble, and ~ 6.5 km in low latitudes (see Fig. 3, horizontal bars). Since in addition to this limitation the retrievals are based on geometric optics we will not interpret the results below 5 km height.

In the lower troposphere advanced retrieval methods based on wave optics are required in order to cope with complex signal structures in the presence of strong refractivity gradients (see e.g., Hocke et al., 1999; Gorbunov, 2002; Sokolovskiy, 2003; Beyerle et al., 2003; Jensen et al., 2003). Wickert et al. (2003b) applied the Full Spectrum Inversion (FSI) technique developed by Jensen et al. (2003) in their study on the comparison of GFZ and IGAM retrievals. Their FSI retrieval results in the lower troposphere may be regarded as complementary to this present study since a comparable data set of the same observation period was used.

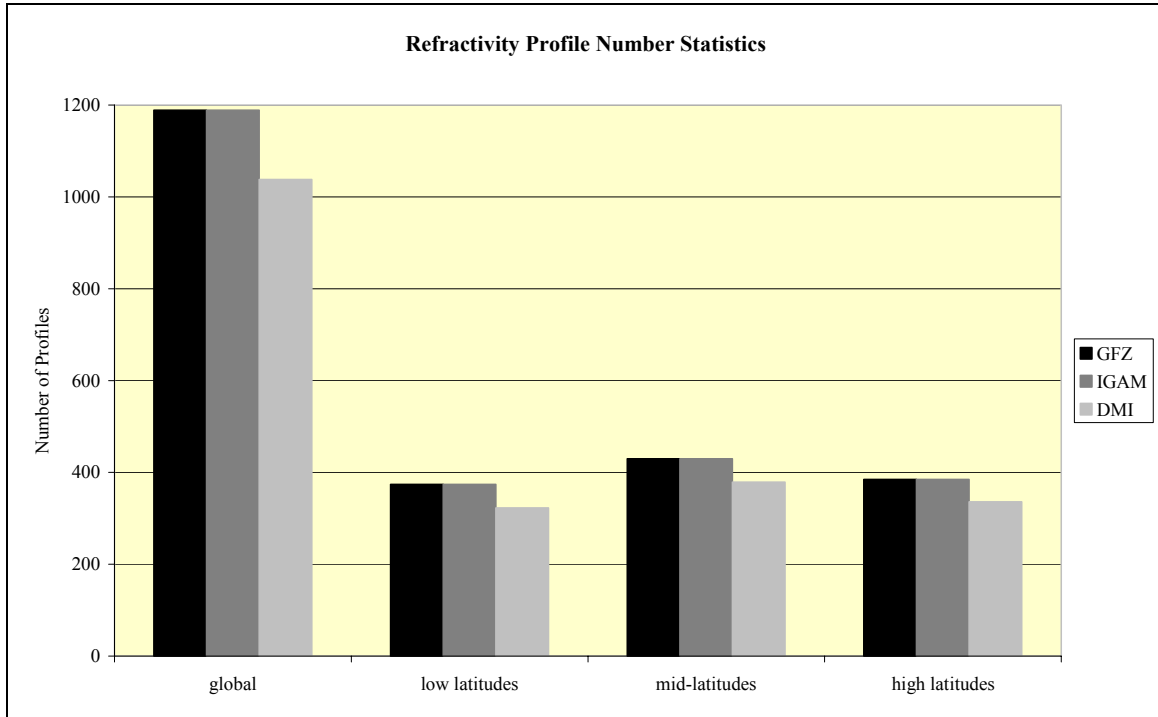


Fig. 2. Comparison of the number of refractivity profiles provided by the GFZ, DMI, and IGAM retrieval scheme for the global and latitudinal data sets, respectively.

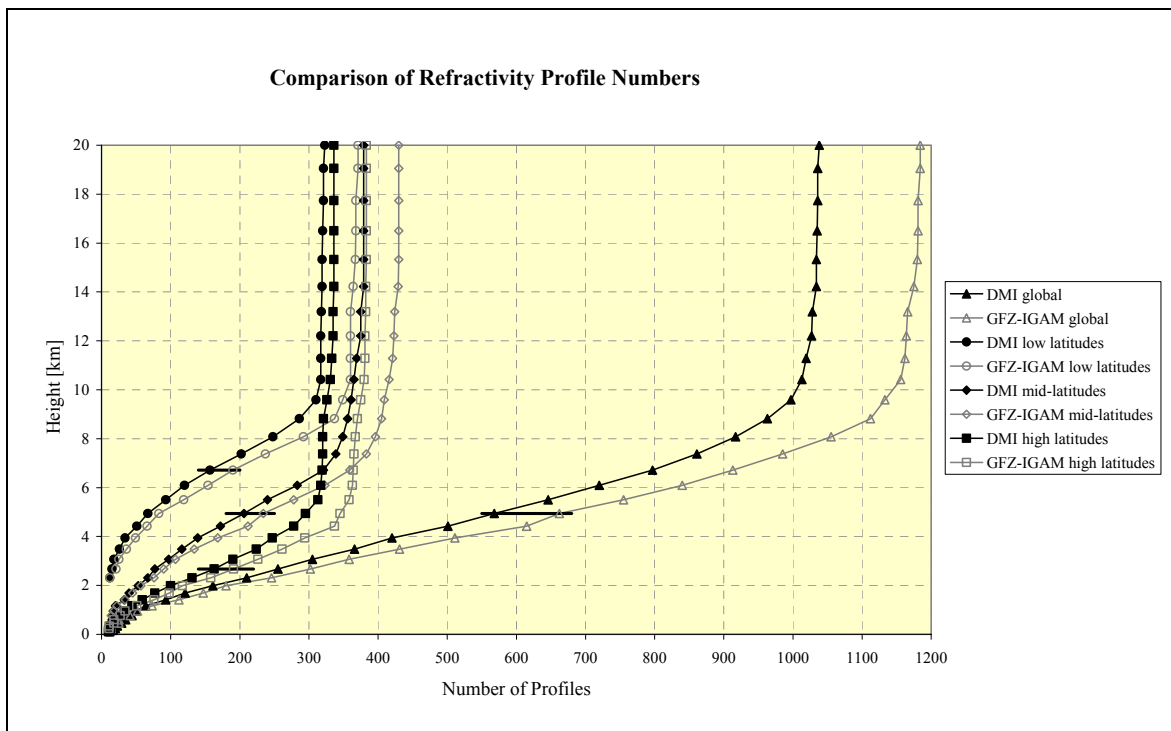


Fig. 3. Number of refractivity profiles provided by the DMI (black), GFZ and IGAM (grey) retrieval scheme for the global (triangles) and latitudinal (low: circles, mid: diamonds, high: square) data sets as a function of height shown up to 20 km, the number of events staying constant above this height. Horizontal bars (thick black lines) indicate the height where the number of profiles is 50% of the respective data set.

3 Statistical Methods

The error statistics is based on the comparison of the retrieved refractivity profiles with colocated refractivity profiles derived from 6 hourly operational meteorological analyses fields from ECMWF. The colocated vertical ECMWF profiles were calculated at a fixed mean tangent point location. When regarding the ECMWF profiles as the truth this implies that the error estimates represent an upper bound error estimate including the observation error, the model (ECMWF) error and the representativeness error. The representativeness error stems from the limited spatial and temporal model resolution and from the comparison of the retrieved profiles with vertical reference profiles. In general, radio occultation profiles are not vertical, the average zenith angle of the tangent point trajectory near the Earth's surface being about 85° . This fact becomes important in the lower troposphere, below ~ 7 km, when high horizontal variability is present (Foelsche and Kirchengast, 2003; Syndergaard et al., 2003). Since we will not interpret results in the lower troposphere the representativeness aspect is negligible in this respect.

The difference profiles ($\Delta \mathbf{x} = (\Delta x_1, \Delta x_2, \dots, \Delta x_i)^T$ with i denoting the height levels and T the matrix transpose) of the retrieved profiles (\mathbf{x}^{retr}) and the "true" profiles (\mathbf{x}^{true}) were calculated at the ECMWF L60 vertical grid.

$$\Delta \mathbf{x} = (\mathbf{x}^{retr} - \mathbf{x}^{true}). \quad (3.1)$$

Calculation of the mean of the difference profiles leads to the bias profile, (\mathbf{b}),

$$\mathbf{b} = \left[\frac{1}{n} \sum_{k=1}^{k=n} \Delta \mathbf{x}_k \right], \quad (3.2)$$

with n being the number of events in the ensemble. Next, the bias was subtracted from each profile giving bias-free profiles ($\Delta \mathbf{x}^{biasfree}$),

$$\Delta \mathbf{x}^{biasfree} = \Delta \mathbf{x} - \mathbf{b}. \quad (3.3)$$

From these bias-free profiles we computed the error covariance matrix (\mathbf{S}),

$$\mathbf{S} = \left[\frac{1}{n-1} \sum_{k=1}^{k=n} (\Delta \mathbf{x}_k^{biasfree})(\Delta \mathbf{x}_k^{biasfree})^T \right], \quad (3.4)$$

with its diagonal elements representing the variances (S_{ii}) at height level i and with its non-diagonal elements representing the covariances (S_{ij}) between height level i and j . The square root of its diagonal gives the standard deviation profile (\mathbf{s})

$$\mathbf{s} \text{ with } s_i = \sqrt{S_{ii}}. \quad (3.5)$$

The root mean square error profiles (\mathbf{rms}) writes

$$\mathbf{rms} \text{ with } rms_i = \sqrt{b_i^2 + s_i^2}. \quad (3.6)$$

The error correlation matrix (\mathbf{R}) with its elements (R_{ij}) denotes the error correlation between Δx_i at height i and Δx_j at height j . It is calculated by dividing the covariances (S_{ij}) by the square root of the variances (S_{ii} and S_{jj}),

$$\mathbf{R} \text{ with } R_{ij} = \frac{S_{ij}}{\sqrt{S_{ii} S_{jj}}}. \quad (3.7)$$

The above described empirical error characteristics were calculated for the data sets of DMI, GFZ, and IGAM for the global and the latitudinal ensembles.

4 Comparison of Retrieval Results

The refractivity error estimates based on the empirical error analyses, described in Sect. 3, are presented for the GFZ (Fig. 4), the DMI (Fig. 5) and the IGAM (Fig. 6) retrieval including the global (panels a) and latitudinal (panels b–d) ensembles. For DMI and IGAM data up to 50 km height are plotted while data of the uppermost boundary levels are not shown. GFZ only provides data up to 35 km height.

The left small panels show the number of events entering the statistics at a given height with the bottom height set at 1 km.

The middle panels illustrate the error characteristics comprising bias, standard deviation, and rms profiles in terms of absolute quantities shown at the upper x-axis and in terms of relative quantities displayed at the lower x-axis. The relative quantities (units %) were computed by dividing the absolute quantities by the mean of the “true” profiles and multiplying with 100. In this paper we will primarily refer to relative quantities. The dotted lines denote the 5 km height level at which all ensembles consist of more than 100 profiles for the calculation of the error statistics. The dotted line at 35 km height indicates the height level below which data from all three retrievals schemes are available. The domain of main interest for the interpretation of the results will be 5–30 km height.

The right panels of Fig. 4–6 display the error correlation functions for different height levels (~40 km, ~30 km, ~20 km, ~10 km, ~5 km) representative of upper stratosphere, lower stratosphere, and troposphere. The error correlation functions are defined as the rows of the error correlation matrix (Eq. 3.7). These functions express the correlation of errors at these heights with the errors in the remainder of the profile and will be discussed in more detail in Sect. 5.

Fig. 4 presents the error statistics results of the GFZ refractivity retrieval compared to ECMWF analyses with the global and mid-latitudinal ensembles showing similar behavior in relative bias (RBIAS) and relative standard deviation (RSTDEV). The RBIAS fluctuates around -0.25% below 25 km and around 0.25% above 25 km height increasing to 0.5% at 35 km height. The RSTDEV is about 0.5–1% at 5–30 km increasing to 2% at 35 km height. In the low latitude ensemble the RBIAS shows larger fluctuations around -0.25% below 20 km height increasing to 0.5% at 28 km height. The RSTDEV stays between 0.5–1% at 8–32 km height increasing to 2% outside this domain. In high latitudes the RBIAS shows small fluctuations around -0.25 to -0.5% below 30 km increasing to 0.75% at 35 km height. The RSTDEV in high latitudes stays between 0.5–0.75% at 5–27 km increasing to 1% at 30 km and to 2.25% at 35 km height.

Results of the DMI refractivity retrieval error statistics are presented in Fig. 5 up to 50 km height and show below the 35 km height level basically the same features and

dimensions in RBIAS and RSTDEV as the GFZ results. Globally, the RBIAS oscillates around -0.3% to -0.2% below 35 km and increases to 3% at 45 km height while the RSTDEV is 0.75–1% below 28 km increasing to 3% at 40 km height. In low latitudes the RBIAS shows again larger fluctuations of -0.5 to 0.5% between 5–35 km height while it keeps oscillating around -0.4% and -0.5% in mid- and high latitudes in this height domain, respectively. The RBIAS increases rapidly to 3% at 40–45 km in mid- and low latitudes and up to 2.5% at 50 km in high latitudes, respectively. The RSTDEV is 0.5–1% at 7–32 km in low latitudes and at 5–28 km in high latitudes whereas it increases in mid-latitudes to 1.5% below the tropopause.

Figure 6 exhibits the results of the IGAM refractivity retrieval in terms of RBIAS and RSTDEV with respect to ECMWF analyses profiles. In the global as well as in the mid- and high latitude ensembles the RBIAS oscillates around -0.4 to -0.5% below 28 km while it ranges from -0.75 to 0.5% in low latitudes. In all ensembles the RBIAS is 0.5% at 35 km increasing to 3% at ~40 km height. The RSTDEV stays below 1% at 5–20 (18) km height in mid- and high (low) latitudes increasing to 1.5% at ~30 km and to 3% at ~40 km height in all ensembles.

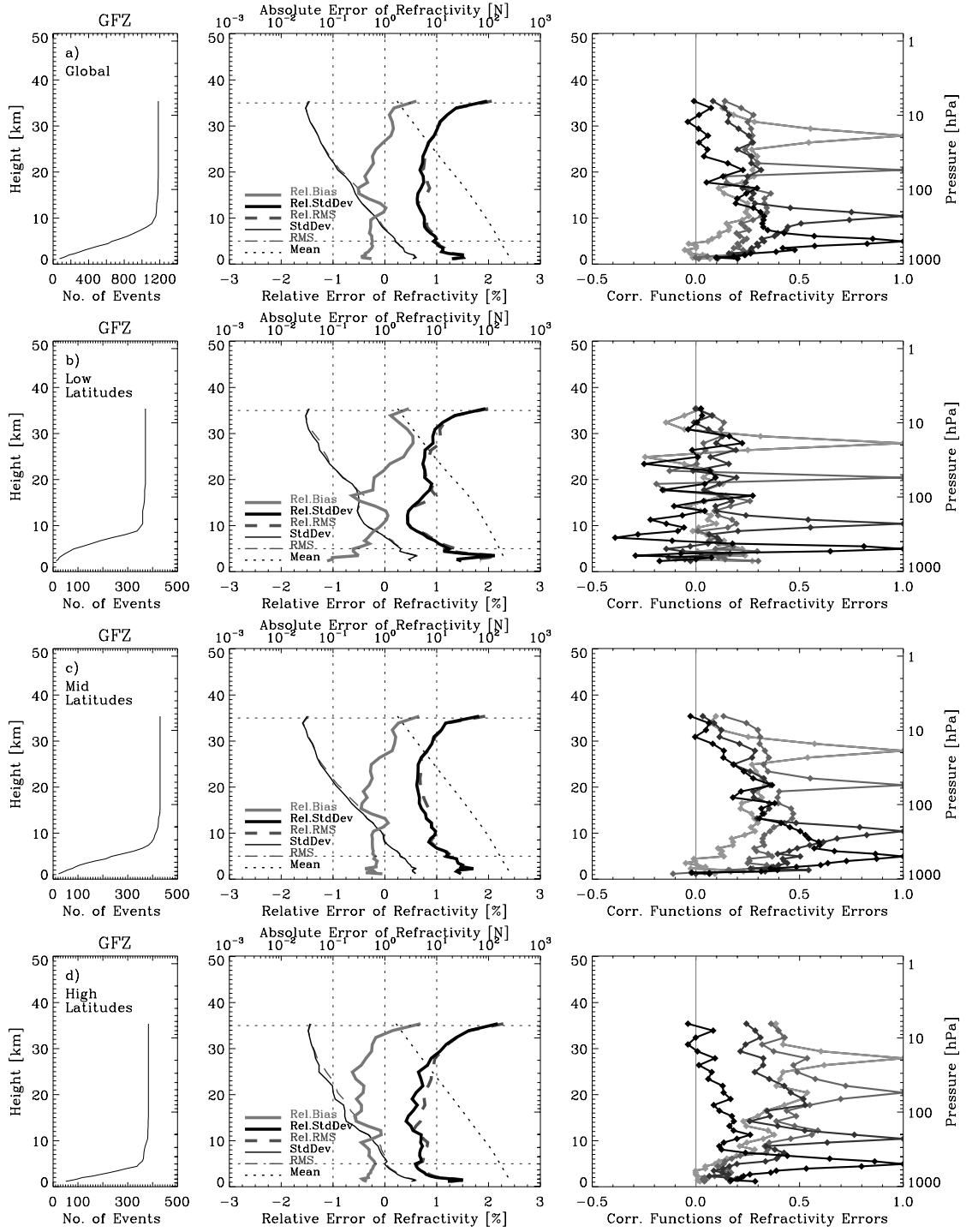


Fig. 4. GFZ – ECMWF refractivity error analysis results for the global (a) and the latitudinal (b–d) ensembles. Left panels: number of events used for the error statistics calculation at any given height. Middle panels: relative bias (heavy grey), relative standard deviation (heavy black), relative rms (heavy dark grey dashed) as well as the absolute standard deviation (light black), absolute rms (light dashed), and the mean of the reference profiles (dotted). Right panels: error correlation functions for ~30 km (light grey), ~20 km (middle grey), ~10 km (dark grey) and ~5 km (black) height, representative of upper stratosphere, lower stratosphere, and troposphere, respectively.

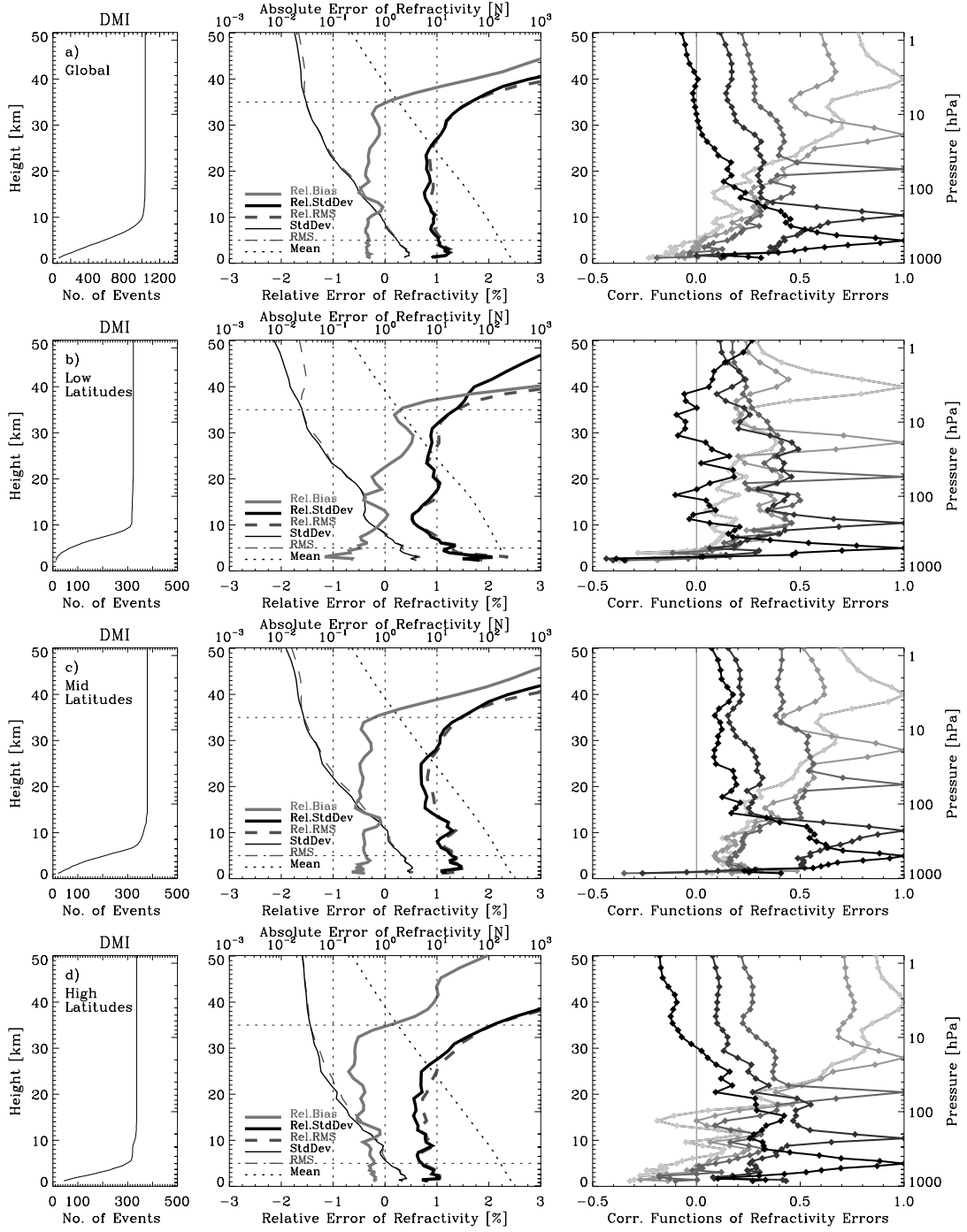


Fig. 5. DMI – ECMWF refractivity error analysis results for the global (a) and the latitudinal (b–d) ensembles. Left panels: number of events used for the error statistics calculation at any given height. Middle panels: relative bias (heavy grey), relative standard deviation (heavy black), relative rms (heavy dark grey dashed) as well as the absolute standard deviation (light black), absolute rms (light dashed), and the mean of the reference profiles (dotted). Right panels: error correlation functions for ~40 km, ~30 km, 20 km, 10 km and 5 km height (ranging from light grey to black), representative of upper stratosphere, lower stratosphere, and troposphere, respectively.

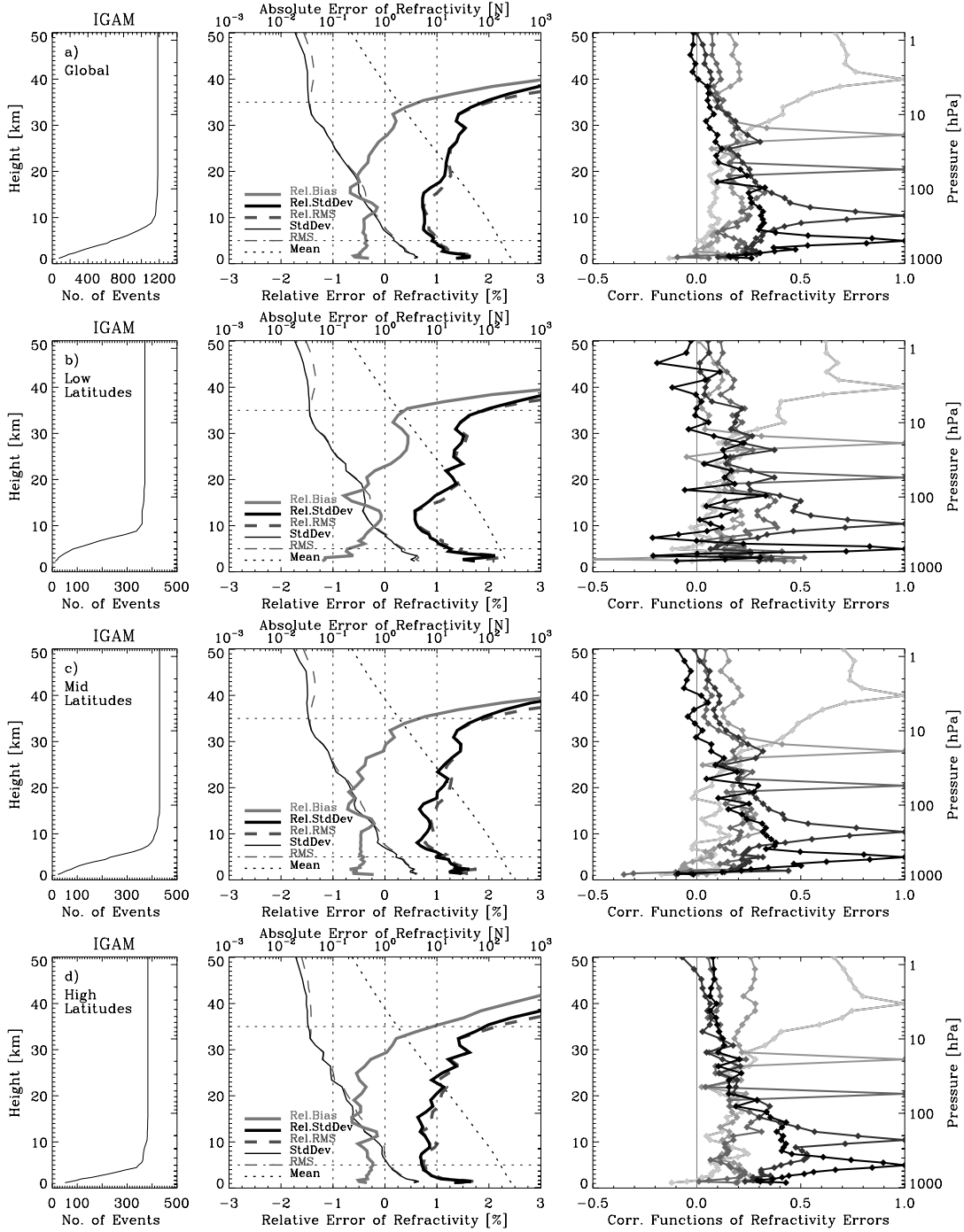


Fig. 6. IGAM – ECMWF refractivity error analysis results for the global (a) and the latitudinal (b–d) ensembles. Left panels: number of events used for the error statistics calculation at any given height. Middle panels: relative bias (heavy grey), relative standard deviation (heavy black), relative rms (heavy dark grey dashed) as well as the absolute standard deviation (light black), absolute rms (light dashed), and the mean of the reference profiles (dotted). Right panels: error correlation functions for ~40 km, ~30 km, ~20 km, ~10 km, and 5 km height (ranging from light grey to black), representative of upper stratosphere, lower stratosphere, and troposphere, respectively.

5 Discussion of Error Characteristics

Basically, the error statistics of all three refractivity retrieval schemes show similar behavior with respect to relative bias and relative standard deviation. Globally, the mean deviation from ECMWF (or relative bias) is about -0.3% at 5–25 km for GFZ and DMI and about -0.4% for IGAM. The relative standard deviation in the global ensembles for GFZ and DMI retrievals ranges from 0.5–1% at 5–30 km height, the relative standard deviation of the DMI retrieval being slightly larger (~0.1%). The IGAM retrieval exhibits a ~0.5% bigger relative standard deviation above ~18 km than GFZ and DMI. This can be addressed to differences in quality control (more conservative at DMI) and to the data processing, most probably the implementation of ionospheric correction and the initialization of bending angles, which is a matter of further retrieval investigations and enhancements. The small negative bias seen in all data sets might partly stem from the allocation of the geometric height vectors between the retrieved and the reference profiles which is also a matter of further investigations.

The GFZ retrieval results are consistent with the data validation performed by Wickert et al. (2003a) who compared ~46,000 CHAMP refractivity profiles to ECMWF analyses and found a mean deviation in refractivity of <0.5% and a relative standard deviation of 0.6–1% at 10–30 km height. Furthermore, the findings of Wickert et al. (2003b) also correspond in terms of relative bias and standard deviation to the GFZ and IGAM retrieval results, since both studies are based on the same observation period.

The differences above ~30 km height in the analyzed retrievals originate from differences in the implemented processing steps and may mainly be due to the bending angle initialization algorithms.

At tropopause heights, a distinct twist especially in the relative bias profiles is present in all ensembles. This feature can be explained with respect to the different height resolution of the radio occultation data and the ECMWF analyses. Since the radio occultation data resolve the tropopause structure on a finer grid than the ECMWF analyses this is displayed in the difference profiles as a twist around the tropopause height which is strongest expressed at the tropical tropopause.

For comparison purposes we present results of an empirical error analysis in Fig. 7. The study is based on simulated (forward-inverse) GNSS radio occultation data (Steiner and Kirchengast, 2003a). The occultation observations were simulated for the planned European weather satellite METOP as Low Earth Orbit satellite and its GRAS receiver as sensor. A forward simulation was performed by raytracing through an ECMWF analyses field and an inverse retrieval was performed. Then the retrieved refractivity profiles were compared to colocated vertical ECMWF profiles which were defined as the truth implying that the error estimates represent an upper bound error estimate including the observation error and the representativeness error. Refractivity exhibits a relative standard deviation of 0.1–0.75% and a relative bias of <0.1% at 5–40 km height. Outside this domain, the relative bias reaches 0.3% in the lower troposphere and up to 0.5% at 50 km. The relative standard deviation stays below 2% outside the 5–40 km domain.

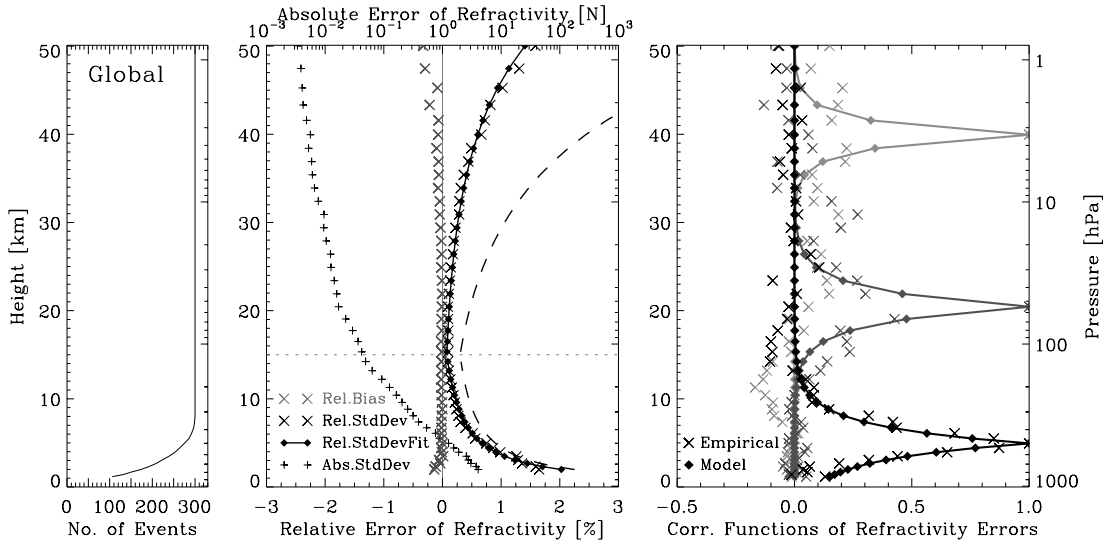


Fig. 7. Refractivity error analysis results of a simulation study for a global ensemble of 300 simulated occultation events. Left panels: number of events used for the error statistics calculation. Middle panels: empirical absolute standard deviation (black crosses), empirical relative bias (grey x), empirical relative standard deviation (black x), as well as the fitted model of standard deviation (black diamonds connected). The dashed line indicates a modeled standard deviation based on a three times bigger error at the tropopause height. Right panels: error correlation functions for ~ 40 km (light grey), ~ 20 km (dark grey), and ~ 5 km (black) height, empirical values (x) and modeled function (connected diamonds).

We tried to deduce simple observation error covariance matrix formulations from the empirical estimated matrices for convenient use in data assimilation systems (Steiner and Kirchengast, 2003b). We used a least squares method for fitting analytical functions to the relative standard deviation which shows a different behavior below and above the tropopause height. We found that the empirical relative standard deviation can be approximated with an exponential increase above the tropopause height (Eq. 5.1) and with a decrease proportional to ‘1/height’ below the tropopause height (Eq. 5.2). The tropopause height is defined globally at 15 km. In order to scale the error magnitude to other than GRAS-type receiver performance we provide these functions with one degree of freedom which is the standard deviation at the tropopause height (*stropo*). Equation 5.1 gives the exponential function for the relative standard deviation (γ) above the tropopause height (z_{tropo}) with the parameter $a = 0.084$ and z representing the height

$$s_{z > z_{tropo}} = stropo * \exp[a(z - z_{tropo})]. \quad (5.1)$$

Equation 5.2 gives the analytical function for the relative standard deviation below the tropopause height with the parameter $b = 4.461$

$$s_{z < z_{tropo}} = stropo + b(z^{-1} - z_{tropo}^{-1}). \quad (5.2)$$

The standard deviation at the tropopause height (*stropo*) is of the order of 0.1 for the empirical study as presented in Fig. 7.

In order to compare the findings of the empirical study with the CHAMP retrieval results we calculated the relative standard deviation based on a three times bigger error at the tropopause height ($stropo = 0.3$) with our model as indicated by the dashed line in Fig. 7. The globally modeled relative standard deviation seems to be a relative good approximation for the behavior of the relative standard deviation especially between 5–

30 km height. Since we do not have yet separated the observation error from the ECMWF model error this might be taken as very conservative upper estimate of the relative standard deviation.

The right panel of Fig. 7 shows the refractivity error correlation functions for three height levels (~ 40 km, ~ 20 km, ~ 5 km) representative of upper stratosphere, lower stratosphere, and troposphere. Refractivity error correlation functions are basically broader than bending angle correlation functions revealing the effect of the Abelian integration. The broadening in the troposphere is mostly a result of the errors due to horizontal variations. Negative correlations in refractivity stemming from derivative operations (Syndergaard, 1999) are most pronounced in low latitudes in lower to middle stratospheric heights. Since the error statistics is performed on an L60 height grid these anti-correlation features are smoothed and can hardly be seen in the global plot but can be resolved on a finer, e.g., L90 grid, which is a matter of current work. The shape of the refractivity error correlation function at an L60 height grid can be approximated by an exponential drop off depending on a correlation length (L) of 2 km in the troposphere linearly decreasing to 1 km at ~ 60 km height. A general refractivity error covariance matrix (S) could then be expressed with the above derived standard deviation

$$S_{ij} = s^2 * \exp\left(-\frac{|z_i - z_j|}{L}\right). \quad (5.3)$$

The refractivity error correlation functions of the CHAMP retrievals with respect to ECMWF are shown in the right panels of Fig. 4–6. The error correlation functions of the IGAM retrieval (Fig. 6) are quite similar to the above described results of the simulation study. The uppermost correlation function at 40 km is very broad with large correlations reflecting the influence of the MSISE-90 background data used for the bending angle initialization. The correlation functions become quite narrow in the stratosphere and show below a broadening due to horizontal variations in the tropospheric region. The same tropospheric and stratospheric behavior is seen in the GFZ (Fig. 4) retrieval. Also the DMI retrieval (Fig. 5) shows these features but the influence of the bending angle initialization seems to reach down below ~ 30 km since larger error correlations are displayed at this height level. A further interpretation of the error correlation function at this stage of investigation cannot be given since an estimation of the ECMWF error correlations in refractivity is necessary in order to make a separation between the model error and the observation error.

6 Summary and Conclusions

An empirical error analysis of CHAMP refractivity retrievals was performed for one week of observations, the data set consisting of about 1200 profiles. Three different data processing schemes were compared and analyzed including the refractivity retrievals of GFZ (Potsdam), DMI (Copenhagen), and IGAM (Graz). The error statistics was based on comparison to reference profiles from ECMWF analyses fields implying that the statistics includes both, the observation error and the ECMWF model error. The results of the refractivity error statistics of CHAMP retrievals were compared to the findings of a simulation study performed for a METOP/GRAS-type observation system (Steiner and

Kirchengast, 2003a; 2003b) and to the results by Kuo et al. (2003) and Wickert et al. (2003a).

The results indicate that the error statistics of all three refractivity retrieval schemes basically show similar features with respect to relative bias, relative standard deviation and error correlation. The relative bias is globally about -0.3% at 5–30 km for GFZ and DMI and about -0.4% for IGAM. The relative standard deviation in the global ensembles ranges from 0.5 to 1% in this height domain. Above 20 km height the IGAM error statistics exhibits a ~0.5% bigger relative standard deviation than the GFZ and DMI error statistics. Differences above ~30 km height originate mainly from the implemented different processing steps including smoothing, ionospheric correction and the bending angle initialization algorithms. This is also obvious in the error correlation functions where the influence of the bending angle initialization gives large correlations as seen in the IGAM retrieval at 40 km, and in the DMI retrieval even below 30 km height. The correlation functions are narrowing in the stratosphere and become broader in the troposphere due to horizontal variations.

Compared to the findings of the simulation study the correlation functions show quite similar features. The relative standard deviation in the simulation study is much smaller than the one in the CHAMP data but it has to be kept in mind that we have not yet separated the observation error from the model error. Nevertheless, we can use the analytical functions deduced from the simulation study and apply it to the CHAMP data set since it has the degree of freedom to adjust for the error magnitude.

We also compared our findings to the results of a study carried out by Kuo et al. (2003). They performed an error analysis with CHAMP and SAC-C data where they tried to separate the observation error from the forecast model error. Our results are consistent with those of Kuo et al. (2003) with respect to the relative standard deviation including both, observation error and ECMWF model error. In order to separate observation from model error Kuo et al. (2003) used the Hollingsworth-Lönnberg method (Hollingsworth and Lönnberg, 1986) which is based on data statistics requiring quite an amount of data in order to give realistic results. They found the observation error of refractivity to be of the order of 0.3–0.5% at 5–25 km increasing to 3% in the tropical lower troposphere but did not investigate the error correlations in their study.

It is of great importance to get also information on the error correlations of ECMWF model errors. Regarding future work we plan to deduce a global error covariance matrix for the ECMWF refractivity model error based on global error estimates of temperature, specific humidity and pressure including vertical error correlations provided by ECMWF. Then we will be able to perform a proper separation of observation error from model error in order to provide realistic observation error covariance matrices for data assimilation systems. Meanwhile, our simple error covariance model deduced from the simulation study results and adjusted to the characteristic error magnitude depending on the respective observing and retrieval system seems to be a quite useful approximation for observation error covariance matrices.

References

- Beyerle, G., J. Wickert, T. Schmidt, and C. Reigber, Atmospheric sounding by GNSS radio occultation: An analysis of the negative refractivity bias using CHAMP observations, *J. Geophys. Res.*, doi:10.1029/2003JD003922, 2003.
- Foelsche, U., and G. Kirchengast, Sensitivity of GNSS radio occultation profiles to horizontal variability in the troposphere: A simulation study, *Proc. 1st Intl. Workshop on Occultations for Probing Atmosphere and Climate*, Sep. 16–20, 2002, Graz, Austria, Springer Verlag, accepted 2003.
- Gobiet, A., and G. Kirchengast, Advancement of GNSS radio occultation retrieval in the upper stratosphere, *Proc. 1st Intl. Workshop on Occultations for Probing Atmosphere and Climate*, Sep. 16–20, 2002, Graz, Austria, Springer Verlag, accepted 2003.
- Gorbunov, M. E., Canonical transform method for processing radio occultation data in the lower troposphere, *Radio Sci.*, 37(5), 1057, doi:10.1029/2000RS002592, 2002
- Healy, S. B., Smoothing radio occultation bending angles above 40 km, *Ann. Geophys.*, 19, 459–468, 2001.
- Healy, S.B., and J. Eyre, Retrieving temperature, water vapour and surface pressure information from refractive index profiles derived by radio occultation: A simulation study, *Q. J. R. Meteorol. Soc.*, 126, 1661–1683, 2000.
- Healy, S. B., A. Jupp, and C. Marquardt, A forecast impact trial with CHAMP radio occultation measurements, paper presented at EGS-AGU-EUG Joint Assembly 2003, Nice, France, April 7–11, 2003.
- Hedin, A. E., Extension of the MSIS thermosphere model into the middle and lower atmosphere, *J. Geophys. Res.*, 96, 1159–1172, 1991.
- Hocke, K., Inversion of GPS meteorology data, *Ann. Geophysicae*, 15, 443–450, 1997.
- Hocke, K., A. G. Pavelyev, O. I. Yakovlev, L. Barthes, and N. Jakowski, Radio occultation data analysis by the radioholographic method, *J. Atmos. Terr. Phys.*, 61, 1169–1177, 1999.
- Hollingsworth, A., and P. Lönnberg, The statistical structure of short range forecast errors determined from radiosonde data. Part I: The wind field. *Tellus*, 38A, 111–136, 1986.
- Jensen, A. S., M. S. Lohmann, H-H. Benzon, and A. S. Nielsen, Full spectrum inversion of radio occultation signals, *Radio Sci.*, 38(3), 1040, doi:10.1029/2002RS002763, 2003.
- Kirchengast, G., End-to-end GNSS Occultation Performance Simulator overview and exemplary applications, *Wissenschaftl Ber 2/98*, IGAM, University of Graz, Austria, 138 pp, 1998.
- Kirchengast, G., J. Fritzer, and J. Ramsauer, End-to-end GNSS Occultation Performance Simulator version 4 (EGOPS4) software user manual (overview and reference manual), Tech. Rep. ESA/ESTEC-3/2002, IGAM, University of Graz, Austria, 472 pp, 2002.
- Kuo, Y.-H., S. V. Sokolovskiy, R. A. Anthes, and F. Vandenberghe, Assimilation of GPS radio occultation data for numerical weather prediction, *Terr. Atmos. and Oceanic Sci.*, 11(1), 157–186, 2000.
- Kuo, Y.-H., T.-K. Wee, S. Sokolovskiy, C. Rocken, W. Schreiner, D. Hunt, and A. Anthes, Inversion and error estimation of GPS radio occultation data, *J. Meteorol. Soc. Japan*, in print 2003.
- Kursinski, E. R., G. A. Hajj, J. T. Schofield, R. P. Linfield, and K. R. Hardy, Observing Earth's atmosphere with radio occultation measurements using the Global Positioning System, *J. Geophys. Res.*, 102, 23,429–23,465, 1997.

- Leitinger, R., J. E. Titheridge, G. Kirchengast, and W. Rothleitner, A “simple” global empirical model for the F layer of the ionosphere, (in German; English version avail. from the authors). *Kleinheubacher Ber.*, 39, 697–704, 1996.
- Ramsauer, J., and G. Kirchengast, Sensitivity of atmospheric profiles retrieved from GNSS radio occultation data to instrumental errors, Tech. Rep. ESA/ESTEC-6/2001, IGAM, University of Graz, Austria, 62 pp, 2001.
- Rieder, M. J., and G. Kirchengast, Error analysis and characterization of atmospheric profiles retrieved from GNSS occultation data, *J. Geophys. Res.*, 106, 31,755–31,770, 2001.
- Steiner A. K., and G. Kirchengast, Ensemble-based analysis of errors in atmospheric profiles retrieved from GNSS radio occultation data, *Proc. 1st Intl. Workshop on Occultations for Probing Atmosphere and Climate*, Sep. 16–20, 2002, Graz, Austria, Springer Verlag, accepted 2003a.
- Steiner A. K., and G. Kirchengast, Empirical error characteristics of radio occultation data for data assimilation systems, paper presented at EGS-AGU-EUG Joint Assembly 2003, Nice, France, April 7–11, 2003b.
- Syndergaard, S., Retrieval analysis and methodologies in atmospheric limb sounding using the GNSS radio occultation technique, DMI Sci. Rep. 99-6, Danish Meteorol. Inst., Copenhagen, Denmark, 131 pp, 1999.
- Syndergaard, S., D. Flittner, R. Kursinski, D. Feng, B. Herman, and D. Ward, Simulating the influence of horizontal gradients on retrieved profiles from ATOMS occultation measurements – a promising approach for data assimilation, *Proc. 1st Intl. Workshop on Occultations for Probing Atmosphere and Climate*, Sep. 16–20, 2002, Graz, Austria, Springer Verlag, accepted 2003.
- Sokolovskiy, S., and D. Hunt, Statistical optimization approach for GPS/Met data inversions, URSI GPS/Met Workshop, Tucson, AZ, 1996.
- Sokolovskiy, S. V., Effect of superrefraction on inversions of radio occultation signals in the lower troposphere, *Radio Sci.*, 38(3), 1058, doi:10.1029/2002RS002728, 2003.
- Vorob’ev, V. V., and T. G. Krasil’nikova, Estimation of the accuracy of the atmospheric refractive index recovery from Doppler shift measurements at frequencies used in the NAVSTAR system, *Phys. of Atmos. and Oceans*, 29, 602–609, 1994.
- Wickert, J., T. Schmidt, G. Beyerle, R. König, C. Reigber, and N. Jakowski, The radio occultation experiment aboard CHAMP: Operational data analysis and validation of vertical atmospheric profiles, *J. Meteorol. Soc. Japan*, accepted 2003a.
- Wickert, J., A. Gobiet, G. Beyerle, A. K. Steiner, U. Foelsche, G. Kirchengast, and T. Schmidt, GPS radio occultation with CHAMP: Comparison of atmospheric profiles from GFZ Potsdam and IGAM Graz, *Proc. 2nd CHAMP Science Meeting*, Sep. 1–4, 2003, Potsdam, Germany, accepted 2003b.

Acknowledgments

The author thanks GFZ Potsdam for the provision of the CHAMP data, especially J. Wickert (GFZ Potsdam) for his cooperation and many fruitful discussions. I am very grateful to A. Gobiet (IGAM, Graz) for the calculation of the IGAM retrievals, the provision of the map plot, for proofreading and for many interesting discussions. C. Marquardt (UKMO, Bracknell) is thanked for providing me with information on model errors. The author is grateful to G. B. Larsen, K. B. Lauritsen, M. Sorensen, X.-Y. Huang, and H. Vedel (DMI, Copenhagen) for their help, for the provision of the DMI retrievals and many discussions on the topic. Last but not least I would like to thank P. Hoeg for his invitation to DMI, F. Rubek for the organization of my stay, and all the colleagues at the DMI/AIR division for a great working atmosphere.

This study was performed in August 2003 during a stay at DMI as a visiting scientist within the GRAS SAF visiting scientist program. The work was financed by the GRAS SAF program. The work was partially funded from the START research award of G. Kirchengast (IGAM, Graz) financed by the Austrian Ministry for Education, Science, and Culture and managed under Program Y103-CHE of the Austrian Science Fund.